

## Numerical Analysis on Liquid JP10 Rotating Detonation Engine

A. Koichi Hayashi\*, Wataru Yoshida<sup>†</sup>, Makoto Asaharai\*\*, Nobuyuki Tsuboi<sup>‡</sup>,

\* Aoyama Gakuin University 5-10-1, Fuchinobe, Chuo-ku, Sagamihara, Kanagawa 252-5258, Japan

<sup>†</sup>Aoyama Gakuin University 5-10-1, Fuchinobe, Chuo-ku, Sagamihara, Kanagawa 252-5258, Japan: Presently ARK Information Systems, INC., Toupure Bldg. 4-2 Gobancho, Chiyoda, Tokyo 102-0076, Japan

\*\* Department of Mechanical Engineering, Gifu University, Gifu, Japan, 501-1193, Japan

<sup>‡</sup> Kyushu Institute of Technology, 1-1, Sensui-cho, Tobata-ku, Kitakyushu, Fukuoka, 804- 8550, Japan

### 1 Introductions

Liquid-gas two phase detonation has not been studied much because of dealing with different phase and complex dynamics although liquid is actual fuel for aerospace vehicles, boat, car, etc. Recently Dabora et al.<sup>[1]</sup> reported that cyclodecane of its diameter of 2.6 mm deforms, breakups, evaporates, mixes, and burns after detonation passes its mixture. Cheatham and Kailasanath<sup>[2]</sup> reported an evaluation of thrust performance of liquid JP10 PDE that specific impulse increases as liquid evaporation rate increases. However there a few work on liquid RDE study. One of the most recent work is presented by Anderson et al.<sup>[3]</sup> to understand liquid injector performance under the transient atmosphere characteristic of RDE. They showed a strong effect of a passing detonation on liquid atomization. In order to get a stable rotating detonation in RDE when liquid fuel is applied, this study will seek the liquid phase influence on rotating detonation structure.

### 2. Numerical method

The two-dimensional compressible Euler equations with the mass conservation equations for each species are used as the governing equations as follows:

$$\begin{aligned} \frac{\partial \mathbf{Q}_g}{\partial t} + \frac{\partial \mathbf{E}_g}{\partial x} + \frac{\partial \mathbf{F}_g}{\partial y} &= \mathbf{S}_g \\ \frac{\partial \mathbf{Q}_l}{\partial t} + \frac{\partial \mathbf{E}_l}{\partial x} + \frac{\partial \mathbf{F}_l}{\partial y} &= \mathbf{S}_l \end{aligned} \quad (1)$$

$$\begin{aligned}
\mathbf{Q}_g &= \begin{bmatrix} \alpha_g \rho_g \\ \alpha_g \rho_g u_g \\ \alpha_g \rho_g v_g \\ \alpha_g \rho_g E_g \\ \alpha_g \rho_{g,i} \end{bmatrix}, & \mathbf{E}_g &= \begin{bmatrix} \alpha_g \rho_g u_g \\ \alpha_g \rho_g u_g^2 + p \\ \alpha_g \rho_g v_g u_g \\ (E_g + p) u_g \\ \alpha_g \rho_{g,i} u_g \end{bmatrix}, & \mathbf{F}_g &= \begin{bmatrix} \alpha_g \rho_g v_g \\ \alpha_g \rho_g u_g v_g \\ \alpha_g \rho_g v_g^2 + p \\ (E_g + p) v_g \\ \alpha_g \rho_{g,i} v_g \end{bmatrix}, & \mathbf{S}_g &= \begin{bmatrix} \dot{m} \\ -F_{D,x} + \dot{m}u_i \\ -F_{D,y} + \dot{m}v_i \\ -[F_{D,x}u_i + F_{D,y}v_i] - Q + \dot{m} \frac{E_l}{\alpha_l \rho_l} \\ \dot{m}_i + \dot{\omega}_i \end{bmatrix} \\
\mathbf{Q}_l &= \begin{bmatrix} \alpha_l \rho_l \\ \alpha_l \rho_l u_l \\ \alpha_l \rho_l v_l \\ \alpha_l \rho_l E_l \\ N_p \end{bmatrix}, & \mathbf{E}_l &= \begin{bmatrix} \alpha_l \rho_l u_l \\ \alpha_l \rho_l u_l^2 \\ \alpha_l \rho_l v_l u_l \\ E_l u_l \\ N_p u_l \end{bmatrix}, & \mathbf{F}_l &= \begin{bmatrix} \alpha_l \rho_l v_l \\ \alpha_l \rho_l u_l v_l \\ \alpha_l \rho_l v_l^2 \\ E_l v_l \\ N_p v_l \end{bmatrix}, & \mathbf{S}_l &= \begin{bmatrix} -\dot{m} \\ F_{D,x} - \dot{m}u_i \\ F_{D,y} - \dot{m}v_i \\ [F_{D,x}u_i + F_{D,y}v_i] + Q - \dot{m} \frac{E_l}{\alpha_l \rho_l} \\ \dot{f} \end{bmatrix} \quad (2)
\end{aligned}$$

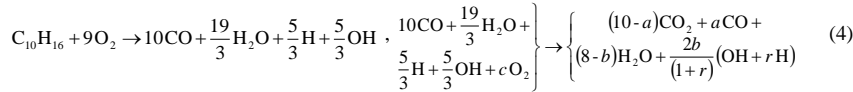
where the physical values between two phases, the drag  $F_d$ , heat transfer  $Q_d$ , evaporation  $\dot{m}$ , droplet increase  $\dot{f}$ , are

$$\begin{aligned}
F_D &= \frac{3}{4} \frac{\alpha_l}{d_l} C_D \rho_g \Delta V (\mathbf{u}_g - \mathbf{u}_l), \quad Q = \alpha_l \rho_l \frac{6Nu C_{pg} \mu_g}{Pr d_l^2} (T_g - T_l), \quad \dot{m} = N_p \frac{12\alpha_l \kappa_g Sh}{C_{pg} d_l^2} \ln(1 + B_{\text{evap}}), \\
\dot{f} &= N_p \frac{\left(\frac{d_l}{d_{lbr}}\right)^3 - 1}{\Delta \tau_{br}} \quad (3)
\end{aligned}$$

In order to integrate the Euler equations, the fluid conservation terms are solved explicitly and the production terms are done implicitly using a point implicit method. The unsteady term is integrated by the third order total variation diminishing Runge-Kutta (TVDRK) method for both phases and the convection terms are solved by the AUSMDV scheme for gas-phase and Hancock scheme for liquid-phase, which are interpolated high-orderly by the second order MUSCL method. In detail the production term is inverted to implicitly decomposed sub-matrices using Gauss-Jordan elimination. In the present analysis it is necessary to calculate a real size of RDE.

## 2.1 JP10 gas-phase reaction model

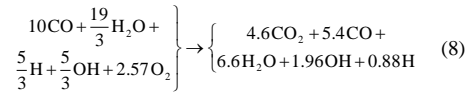
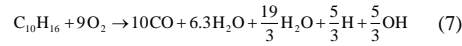
In order to evaluate a RDE analysis using JP10, we need an appropriate reaction model of JP10. It is known from the past studies that combustion chamber size affects thrust performance of RDE. Hence it is necessary to use the same numerical combustion chamber size for all numerical calculation cases while considering the real RDE chamber. It is inadequate to calculate a real size RDE with a big detailed reaction model<sup>[4]</sup> and with a large number of grids. A two-step reduced reaction model of gaseous JP10 proposed by Varatharajan et al.<sup>[5]</sup> is used in the present calculation. Although JP10 is liquid at the standard temperature and pressure, the liquid evaporation is not considered, but as previously described, the gaseous JP10 is considered in the present analysis. The following equations explain the detail of two-step JP10 reaction system:



$$\begin{aligned}
 a &= 10/(1+k_{5\infty}/k_{6\infty}) \\
 b &= 8(1+r)/(1+r+2\sqrt{rs}) \\
 \text{where } c &= (10-a)/2 + b(1-r)/(2(1+r)), \quad (5)
 \end{aligned}$$

$$\begin{aligned}
 r &= C_{H,\infty}/C_{OH,\infty} \\
 s &= k_{3\infty}C_{H_2O,\infty}/k_{4\infty} \\
 k_{\infty} &= AT_{\infty}^n \exp(-E_a/RT_{\infty}), \quad C_i = \rho X_i/W \quad (6)
 \end{aligned}$$

Equations (4) are the overall chemical reaction mechanisms and Equations (5) are the equations of coefficients used in Equations (4), where  $k$  is the reaction constant,  $C_i$  is the mole concentration, and  $\infty$  implies the equilibrium state. The equilibrium temperature,  $T_{\infty}$ , and the mole concentration of each chemical species,  $C_i$ , are obtained using the CHEMKIN program, then the coefficients,  $a$ ,  $b$ , and  $c$ , in the chemical reaction equations, (4), can be obtained from these  $T_{\infty}$  and  $C_i$  after calculating the equilibrium temperature,  $T_{\infty}$ .



## 2.2 Validation of the two-step reaction model

Figures 1 and 2 show the relation between the pressure and the equivalence ratio,  $\phi$  and that between the temperature and the equivalence ratio, respectively, where the blue solid circle and solid triangle are calculated using the detailed chemical reaction model and the orange solid circle and red solid triangle are done using the two-step reduced reaction model. As described in the previous paragraph, the ZND value is at the detonation front or just behind the detonation front and the CJ value is at the equilibrium state far behind the detonation front. In Fig.1  $p_{ZND}$  increases as  $\phi$  increases, but  $p_{CJ}$  decreases as  $\phi$  increases because the velocity increases. In Fig.1 there is not much change in  $T_{ZND}$  for the equivalence ratio  $\phi$ , but is some increase in  $T_{CJ}$  for the increase of  $\phi$  because the energy increases. The maximum differences between these values by the detailed reaction mechanism and that by the two-step reduced reaction mechanism for  $p_{ZND}$ ,  $T_{ZND}$ ,  $p_{CJ}$ , and  $T_{CJ}$  are 12.4%, 11.0%, 9.57%, 7.08%, respectively. From those results the original program used in the present study will be valid to calculate JP10-air RDE.

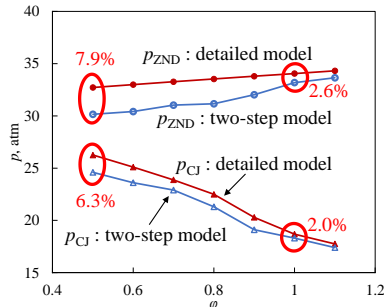


Fig.1 Pressure vs equivalence ratio for using the two-step chemical reaction model and the detailed chemical reaction model.

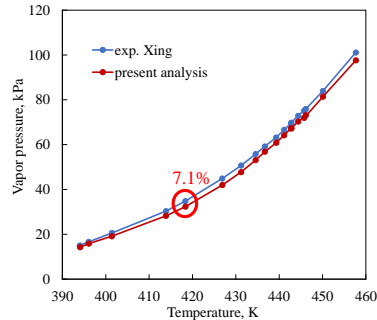


Fig.2 Comparison of vapor pressure between Xing's experimental data[6] and the present numerical ones.

Fig.2 shows a comparison of vapor pressure between Xing's experimental data [6] and the present numerical ones. A qualitative similarity is observed in the figure and the maximum difference between the numerical results and experimental one is about 7.1 % at the temperature of 418 K. From these results the present numerical code for JP10/air two-phase Euler system seems to give a reasonable physics for the liquid RDE calculation.

### 3. Analysis of rotating detonation engine

#### 3.1 Numerical conditions

Two-dimensional RDE is calculated using the two-phase Euler equations with the two-step JP10/air reaction mechanism. The combustion chamber size is 63.7 mm in diameter, 50 mm in the flowing axis direction based on the Kindracki's experiment[7]. The grids are equally-spaced to be 100  $\mu\text{m}$  and the number of grids is 501x2001. The boundary conditions are that the left boundary is a flow-in wall of JP10/air mixture; the right boundary is flow-out condition; and the top and bottom boundaries are a periodic condition. There are many micro-Laval nozzles are set at the boundary between the storage tank and combustion chamber. The fuel is JP10 and the oxidiser is air. The equivalence ratio of mixture is 1.0. The storage tank pressure is kept 2 Mpa and its temperature is 460 K. In the present study the evaporation rate  $\eta$  from 20 to 80 % and the droplet diameters  $d_i$ , 1 and 5  $\mu\text{m}$  are changed to study on their effects on detonation behaviour.

### 4. Results and discussion

The pressure and temperature profiles in the combustion chamber, the JP10 mass fraction and liquid-phase profiles, the dynamic process of unreacted pockets and transverse waves, the generation mechanism of unreacted pockets and the quenching mechanism of rotating detonation are discussed. However the quenching mechanism of rotating detonation is shown in the present extended abstract to shorten the discussion.

It is necessary to drive rotating detonation steadily for a real rotating detonation engine. For the purpose of such continuous drive, we have to know the limit and mechanism of quenching detonation for liquid RDE. Because the present study deals with a relatively large grid size (maybe ok for liquid detonation case due to its large cell size) and a two-step reaction mechanism, we cannot discuss the rotating detonation in very detail. Since rotating detonation with zero evaporation rate gives no rotating detonation propagation and its quench, the following discussion will be given using zero evaporation case of rotating detonation.

The previous studies in our laboratory showed that (i) to maintain RDE it is necessary for a generation of transverse detonation (Yamada et al. [8]) and (ii) it is observed that a transverse detonation is newly generated at the downstream end of detonation front (Uemura et al. [9]). In the present study of JP10/air RDE simulation we

コメントの追加 [AKH1]:

found out the similar transverse wave generation at the downstream side of the detonation front. Without this transverse detonation generation RDE will not be continued to provide thrust to the aerospace flight. In the limit case of zero % evaporation the rotating detonation head disappears after the transverse wave extincts at the downstream side of the detonation front.

Fig.3 shows the extinction process of RDE detonation front for pressure profiles and temperature profiles. At Fig.3-(a) the detonation front has a nice and strong pressure and temperature profile. The white circle in the temperature profile is the place where a new transverse wave appears. Fig.3-(b) shows that the pressure profiles become lower than the case of Fig.3-(a). We can recognize the transverse waves are moving left and right as the arrows show their direction. However the temperature profiles do not show much difference from that of Fig.3-(a). Fig.3-(c) shows that the directions of transverse waves moving are all right direction and the new transverse detonations are not generated at the downstream edge of the detonation front. As far as temperature profiles, Fig.3-(d) shows the detonation front is distracted in the red circle region of the pressure profiles. While the temperature profiles the temperature becomes very low at the white arrow area. This is the detonation head failure where the fresh fuel flows in the detonation front. Fig.3-(e) shows that the detonation front is almost completely distinguished in the pressure profiles, while there is still a hot region existed in the temperature profiles. The amount of fresh mixture's flowing into the detonation front is increasing at this moment.

As a summary,

- (1) The transverse detonation is not generated at the downstream end of detonation front and the pressure at the detonation front becomes low.
- (2) There disappear the transverse waves moving towards the injection side of the wall and all transverse waves move to the downstream.
- (3) The detonation front becomes disappearing at the fuel injection side and the fresh mixture makes pressure and temperature down.
- (4) All the transverse waves are moving towards downstream to extinguish the detonation front.

## 5. Conclusions

The present extended abstract shows the numerical analyses of the JP10/air two-phase detonation physics for the purpose to get a stable performance of detonation engine. We obtained the following understandings for the JP10/air two-phase detonation, which including the results not describing in this manuscript:

- (1) When the evaporation rate increases, because of decreasing the gas-phase energy loss, 1D-detonation limit of pressure  $p_{ZND}$ , temperature  $T_{ZND}$  and the Chapman-Jouguet pressure  $p_{CJ}$  and  $T_{CJ}$  increase.
- (2) When the fuel droplet diameter  $d_l$  becomes small, the area of interface between gas and droplet surface increases and its vaporization rate becomes faster, then the interface pressure  $p_{ZND}$  and temperature  $T_{ZND}$  become low.
- (3) The unreacted pockets appear at the condition of the evaporation rate of 20 % and lower for RDE.
- (4) For the case of the evaporation rate of 0 %, the transverse wave does not generated at the downstream side of detonation front and the detonation becomes extinguished.

## References

- [1] Dabola, E.K, Ragland, K.W., and Nicholls, J.A., Proc. Of the Comb. Inst. Vol.12 (1969) 19-26
- [2] Cheatham, S. and Kailasanath, K., AIAA J. 43, 6 (2005) 1276-1283.
- [3] Anderson, W.S., Lim, D., Washington, M.R., Heister, S.D., 55<sup>th</sup> AIAA Aerospace Science Meeting, Grapevine, Texas, AIAA Paper 2017-1932.
- [4] Li, S. C., B. Varatharajan., and F. A. Williams, "Chemistry of JP-10 Ignition", AIAA Journal, 39 (2001), 2351-2356.
- [5] Varatharajan, B. and Petrova, M., Williams, F.A., and Tangirala, V., "Two-step chemical-kinetic descriptions for hydrocarbon-oxygen-diluent ignition and detonation applications", Proceedings of the Combustion Institute, 30 (2005), 1869-1877.

- [6] Xing, Y., Fang, W., Li, D., Guo, Y., and Lin, R., "Density, Viscosity, and Vapor Pressure for Binary Mixtures of Tricyclo [5.2.1.0<sup>2,6</sup>] Decane and Diethyl Carbonate", *Journal of Chemical and Engineering data*, 54 (2009), 1865-1870.
- [7] Kindracki, J., Wolanski, P., and Gut, Z., *Shock waves* 21 (2011) 75-84.
- [8] Yamada, T., Hayashi, A.K., Yamada, E., Tsuboi, N., Tangirala, V.E., and Fujiwara, T., "Numerical Analysis of Threshold of Limit Detonation in Rotating Detonation Engine," AIAA 2010-0153, 48th AIAA Aerospace Sciences Meeting, Orlando, FL., January 2010.
- [9] Uemura, Y., Hayashi, A. K., Asahara, M., Tsuboi, N., and Yamada, E., "Transverse Wave Generation Mechanism in Rotating Detonation," *Proceedings of the Combustion Institute*, Vol. 34, No. 2, 2013, pp. 1981- 1989.

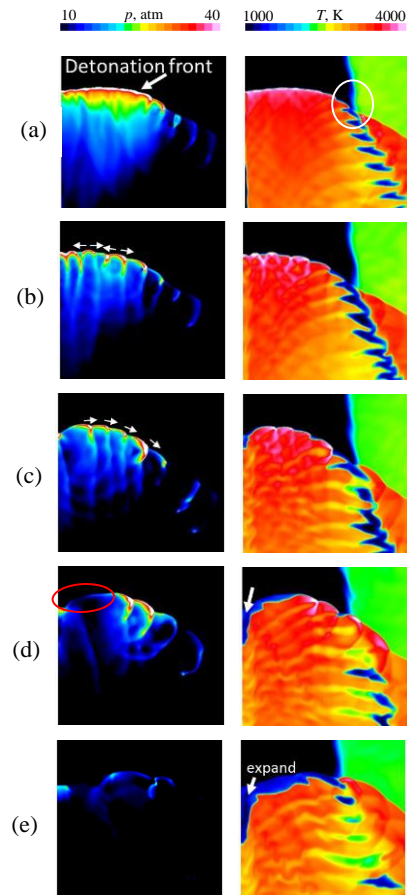


Fig. 3 The process of liquid JP10/air detonation front extinction.